Lawrence Berkeley National Laboratory

LBL Publications

Title

Guest-, Light- and Thermally-Modulated Spin Crossover in [FeII2] Supramolecular Helicates

Permalink

https://escholarship.org/uc/item/21p4m46p

Journal

Chemistry - A European Journal, 22(25)

ISSN

0947-6539

Authors

Darawsheh, Mohanad

Barrios, Leoni A

Roubeau, Olivier

et al.

Publication Date

2016-06-13

DOI

10.1002/chem.201601080

Peer reviewed

eScholarship.org Powered by the California Digital Library
University of California

Guest, Light and Thermally Modulated Spin Crossover in [Fe(II)$_2$] Supramolecular Helicates

ChemSusChem
Full Papers

M. Darawsheh,[a] L. A. Barrios,[a] O. Roubeau,[b,*] S. J. Teat[c] and G. Aromí[a,*]

Abstract: A new bis–pyrazolylpyridine ligand (H_2L) has been prepared to form functional $[Fe_2(H_2L)_3]^{4+}$ metallohelicates. Changes to the synthesis yield six derivatives; $X@[Fe_2(H_2L)_3]Cl(PF_6)_2{\cdot}xCH_3OH$ (**1**, x=5.7 and X=Cl; **2**, x=4 and X=Br), $X@[Fe_2(H_2L)_3]Cl(PF_6)_2{\cdot}yCH_3OH{\cdot}H_2O$ (**1a**, y=3 and X=Cl; **2**, y=1 and X=Br) and $X@[Fe_2(H_2L)_3](I_3)_2{\cdot}3Et_2O$ (**1b**, X=Cl; **2b**, X=Br). Their structure and functional properties are described in detail *via* single crystal X-ray diffraction (SCXRD) experiments at several temperatures. **1a** and **2a** are obtained from **1** and **2**, respectively, *via* single-crystal-to-single-crystal (SCSC) mechanisms. The three possible magnetic states, [LS–LS], [LS–HS] and [HS–HS] can be accessed over large temperature ranges, thanks to the structural non-equivalence of the Fe(II) centres. The nature of the guest (Cl^- *vs* Br^-) shifts the SCO temperature by *ca.* 40 K. Also, metastable [LS–HS] or [HS–HS] states are generated through irradiation. Helicates $(X@[Fe_2(H_2L)_3])^{3+}$ persist in solution.

Introduction

The phenomenon of spin crossover (SCO) may be encountered for transition metals that exhibit two possible distributions of the electrons among their crystal field split *d* orbitals, if both configurations are sufficiently close in energy.[1] By far, the most commonly studied case is that of octahedral Fe(II) ions, which may switch between a diamagnetic (S = 0, low spin, LS) and a paramagnetic state (S = 2, high spin, HS).[2] The switching comes about by means of external stimuli,[3] such as changes to the temperature[4] or pressure,[5-6] light irradiation,[7] or modulation of the crystal field near the metal by secondary components not directly bound to it.[8-10] The spin transition (ST) is accompanied by drastic changes to the physical properties of the material (optical, magnetic, electrical, etc.) also affecting the structure, which converts these systems into very promising candidates for the implementation of functional/switchable nanoscopic devices.[11] The tools and concepts developed in coordination supramolecular chemistry[12-13] could be very beneficial for exploiting the SCO at the molecular scale. One particular challenge is designing molecular systems featuring more than one spin active center with spin states controllable by means of external stimuli. A pioneering example was a molecular grid of four Fe(II) centers made with a specially designed ligand. This assembly could be brought to three different HS/LS state combinations of its metals by using light irradiation or by controlling the temperature.[14] In this context, a well-known family of coordination architectures that can be very useful are the so called metallohelicates.[15] These species are amenable to rational design; the right choice of metals and polydentate ligands allows the prediction and formation of helicates with different numbers of metals and strands.[16-17] In addition, with the right choice of ligand donors, it is possible to chemically tune the crystal field around the metals (e.g. Fe(II)) of the supramolecular assembly in order to facilitate the occurrence of SCO.[18-22] Some of the reported examples show evidence that the spin active centers can be brought from the LS to a metastable HS state in response to light irradiation, via the LIESST (light induced excited state trapping) effect.[23] With a more sophisticated design of ligands, metallohelicates are also amenable to selectively capture guest species inside them,[24-27] which offers a valuable opportunity for modulating the functional properties of their components such as the switching behavior of potential SCO metals. **In fact, such a tuning of the SCO behavior through encapsulation of guests is extremely rare in supramolecular chemistry, and when encountered, it has indeed led to only very minor effects.[28]**

We present here a new bis–pyrazolylpyridine ligand (H_2L, Scheme 1) designed for the formation of Fe(II) metallohelicates. **Bis–pyrazolylpyridine ligands have indeed been used successfully in the past for the preparation of coordination cages,[29] including Fe(II) helicates.[30]** Ligand H_2L well suited to facilitate the encapsulation of anionic guests; the molecular structure of several $(X@[Fe_2(H_2L)_3])^{3+}$ complex cations are thus presented (X^- = Cl^-, Br^-). The donor properties of H_2L confer the metals the capacity of undergoing thermal SCO at temperatures that are modulated by the guest in a quite significant manner (in the solid state as well as in solution). The specific composition in the solid state offers the possibility to discriminate structurally each metal of the dinuclear assembly and observe a different magnetic behavior for each of them. Thus the three possible magnetic states, [LS–LS], [LS–HS] and [HS–HS] may be observed and stabilized over large temperature ranges, by playing with the chemical variables. The latter include solid state solvate exchange processes with the atmosphere occurring in single-crystal-to-single-crystal (SCSC) manner and monitored by single crystal X-ray diffraction (SCXRD). Some of the above magnetic states can also be accessed as metastable light-induced phases at low temperature.

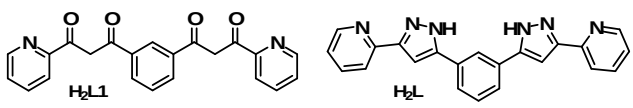

Scheme I. Molecular drawings of compounds H_2L1 and H_2L.

[a] Mr. M. Darawsheh, Dr. L. A. Barrios, Dr. G. Aromí
Departement de Inorgánica, Universitat de Barcelona, Diagonal 645, 08028, Barcelona, Spain. E-mail: guillem.aromi@qi.ub.es

[b] Dr. O. Roubeau
ICMA, Instituto de Ciencia de Materiales de Aragón (ICMA), CSIC and Universidad de Zaragoza, Plaza San Francisco s/n, 50009, Zaragoza, Spain.E-mail: roubeau@unizar.es

[c] Dr. S. J. Teat
Advanced Light Source, Berkeley Laboratory, 1 Cyclotron Road, Berkeley, California 94720, USA.

WILEY

Results and Discussion

Synthesis

The bis-*β*-diketone H_2L1 (Scheme I) was prepared through a common Claisen condensation between a ketone and an ester (Fig. S1), as previously reported for other related ligands.[31] This species served as precursor of the bis–pyrazolylpyridine ligand H_2L (Scheme I), accessed through a double ring closure following its reaction with hydrazine (Fig. S1). This bis-chelating ligand could potentially form helicates, furnish an appropriate environment to Fe(II) for the SCO and encapsulate anions *via* N−H···X hydrogen bonds. The reaction in methanol of FeX_2 (X=Cl, Br) salts with H_2L in the presence of Bu_4NPF_6 (the latter as a source of a counterion) leads indeed to crystallization of the assemblies $X@[Fe_2(H_2L)_3]X\cdot(PF_6)_2$ (de-solvated **1** and **2** for Cl and Br, respectively) consisting of cationic triple stranded Fe(II) dinuclear helicates, encapsulating one X^- anion. Upon prolonged exposure to air, crystals of **1** and **2** experience the exchange of guest lattice molecules producing **1a** and **2a**. The latter are thus solvathomorphs of **1** and **2** after losing 2.7 or 3 molecules of MeOH, respectively, and absorbing one equivalent of H_2O. Transformations **1** → **1a** and **2** → **2a** remarkably occur in a single-crystal-to-single-crystal (SCSC) manner, thus allowing the full structure determination of both resulting products. Attempts to encapsulate the larger halide I^- by employing the salt FeI_2 in the original reaction led to crystallization from Et_2O of the novel compound $Cl@[Fe_2(H_2L)_3](I_3)_3\cdot3Et_2O$ (**1b**) in very low yield, with Cl^- arising from a trace impurity. The anion I_3^- was the result of aerobic oxidation of I^-, which is not rare in inorganic chemistry.[32] The reaction was then optimized by using the $FeCl_2$ salt and introducing excess iodide as Bu_4NI, although the yield of the crystallized compound remained quite small, most likely due to low concentrations of the *in situ* formed I_3^- anions. The same procedure could be then replicated with Br^-, with the convenient formation of $Br@[Fe_2(H_2L)_3](I_3)_3\cdot3Et_2O$ (**2b**), although again in moderate yields. The inability to encapsulate I^- is thought to be due to the large volume of this anion, exceeding the space available inside the $[Fe_2(H_2L)_3]^{4+}$ host, as could be ascertained by analyzing the molecular structure of the helicates (see below). **A summary of the six derivatives prepared with their main features is in Table 1, to facilitate the reading.**

Description of Structures

$Cl@[Fe_2(H_2L)_3]Cl\cdot(PF_6)_2\cdot5.7CH_3OH$ (1). Compound **1** is found at 100 K in the tetragonal space group $I4_1cd$ (Tables S1 and S6). The asymmetric unit consists of one helical $[Fe_2(H_2L)_3]^{4+}$ complex cation with an encapsulated Cl^- anion (Fig. 1), together with an external Cl^- and two PF_6^- ions, in addition to five full solvent MeOH molecules, and one with 70% occupancy. Of the solvent molecules, three are disordered over two positions, as well as one of the PF_6^- anions. The unit cell encloses a total of sixteen such ensembles. The cationic helicate (Fig. 1) is formed by two Fe(II) metal centers defining the central axis and three H_2L ligands acting as strands. The latter chelate both metals through their pyrazolyl-pyridine moieties (each approximately confined in one plane) completing distorted chiral six-coordination around them. In this manner, each helicate in the lattice displays either *ΔΔ* or *ΛΛ* metal configuration sets, leading to enantiomeric species, present as racemic mixtures in the crystal by virtue of its group symmetry.

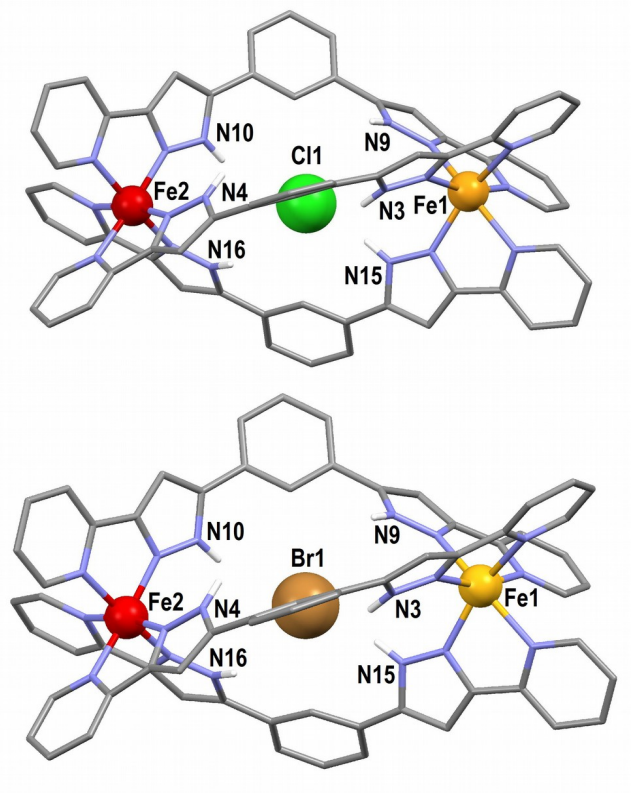

Figure 1. Molecular representation of the cationic species $(X@[Fe_2(H_2L)_3])^{3+}$ (X=Cl, **1**, top; Br, **2**, bottom) at 100 K, emphasizing the spin state of the Fe(II) ions at this temperature, showing the *ΔΔ* configuration (see text). Only hydrogen atoms on N atoms are shown (white). Color code: grey, C; purple, N; orange, HS Fe(II); red, LS Fe(II); green Cl; turquoise, Br. For complex **1/2**, Fe, Cl/Br and the N atoms involved with intermolecular interactions with Cl/Br are labelled.

Table 1. Summary of compounds 1, 2, 1a, 2a, 1b and 2b and of their main distinctive features.

Num.	formula	space group	spin 100 K	states 300K	T_{SCO} (K)
1	$Cl@[Fe_2(H_2L)_3]Cl\cdot(PF_6)_2\cdot 5.7CH_3OH$	$I4_1cd$	[LS–HS]	[HS–HS]	302.1(3)
2	$Br@[Fe_2(H_2L)_3]Br(PF_6)_2\cdot 4CH_3OH$	$I4_1cd$	[LS–HS]	[HS–HS]	258.2(3)
1a	$Cl@[Fe_2(H_2L)_3]Cl(PF_6)_2\cdot 3CH_3OH\cdot H_2O$	$I4_1acd$	[LS–LS]	[HS–HS]	185.0(3)/258.9(3)
2a	$Br@[Fe_2(H_2L)_3]Br(PF_6)_2\cdot MeOH\cdot H_2O$	$I4_1acd$	[LS–LS]	[HS–HS]	≈200
1b	$Cl@[Fe_2(H_2L)_3](I_3)_3\cdot 3Et_2O$	$R\bar{3}$	[HS–HS]	[HS–HS]	--
2b	$Cl@[Fe_2(H_2L)_3](I_3)_3\cdot 3Et_2O$	$R\bar{3}$	[HS–HS]	[HS–HS]	--

The chloride encapsulated by the helicate is held within the cavity through six hydrogen bonding interactions with the N–H groups of the pyrazolyl moieties (Fig S2). Of these, two are clearly stronger than the rest (Tables 2 and S11), which causes the Cl^- anion to be closer to one iron center (Fe1) than to the other by 0.33 Å.

Table 2. Interatomic distances (Å, T = 100 K for **1**/**2** and **1b**/**2b** and T = 90 K for **1a**/**2a**) involving the encapsulation of a halide ion X^- (X=Cl, Br) within complexes **1**, **2**, **1a**, **2a**, **1b** and **2b**.

	1/2	1a/2a	1b/2b
N3–H···X1	3.2144(5)5/3.362	3.377(7)/3.39	3.542(3)/3.50
Fe1···X1	4.698(2)/4.789(2)	4.838(6)/4.847(1)	5.036(1)/4.938(1)
Fe2···X1	5.038(2)/4.883(2)	~~4.838~~/~~4.847~~	4.768(1)/4.824(1)

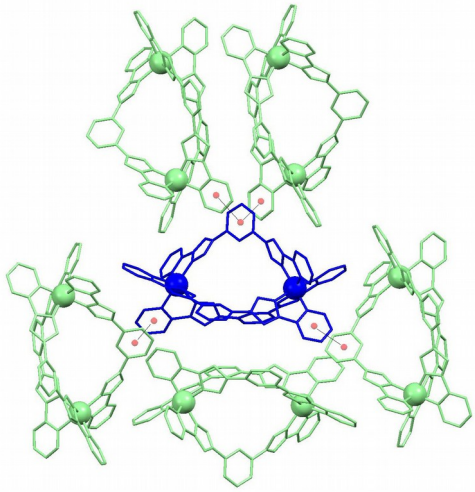

The external Cl^- group is located next to the complex cage, establishing one hydrogen bond with an N–H group, also near Fe1, and one molecule of methanol (Fig. S2). Thus the Fe atoms in **1** differ on the nature of the species forming hydrogen bonds with their β-N–H groups. The N–H groups adjacent to Fe1 act as donors to Cl^- ions, whereas the N–H moieties near Fe2 interact with the oxygen atom of MeOH molecules. These differences translate into two distinct magnetic responses (see below), which at 100 K causes Fe1 to be in the high spin (HS) state while Fe2 is low spin (LS). This is reflected in the metric parameters around these ions, such as the average Fe–N bond distances, $\langle d_{(Fe\text{-}N)}\rangle$, of 2.190 and 1.980 Å for Fe1 and Fe2, characteristic of their respective spin states.[33] These observations confirm the established fact that out-of-sphere intermolecular interactions are crucial to the magnetic state of SCO centers.[34-35] Here, hydrogen bonds of the N–H groups towards Cl^- stabilize the HS state more than the interactions with MeOH molecules. **These results are to be compared with a previously reported $[Fe(II)_2]$ helicate, with a bis-(imidazolimine) ligand,[22] which shows the same magnetic dissimilarity between both metals of the molecule. In that case, the differing behavior is explained by the presence of a strong π···π contact, near one of the Fe(II) centers, perhaps restraining the structural changes related to a process of SCO**. The supramolecular $(Cl@[Fe_2(H_2L)_3])^{3+}$ species are organized in sheets parallel to the crystallographic *ab* plane (Fig. S3), mutually connected through π···π and C–H···π interactions involving some of their numerous aromatic rings, where each helicate sees five related first neighbors (**Fig. 2**). These sheets, described as hydrophobic because of the organic ligands, intercalate with hydrophilic layers composed of the external Cl^- and PF_6^- ions and MeOH molecules (Fig. S3).

The space occupied by the layers of anions and solvents seems appropriate for polar molecules to diffuse and exchange with other such molecules from the environment. This seems to be

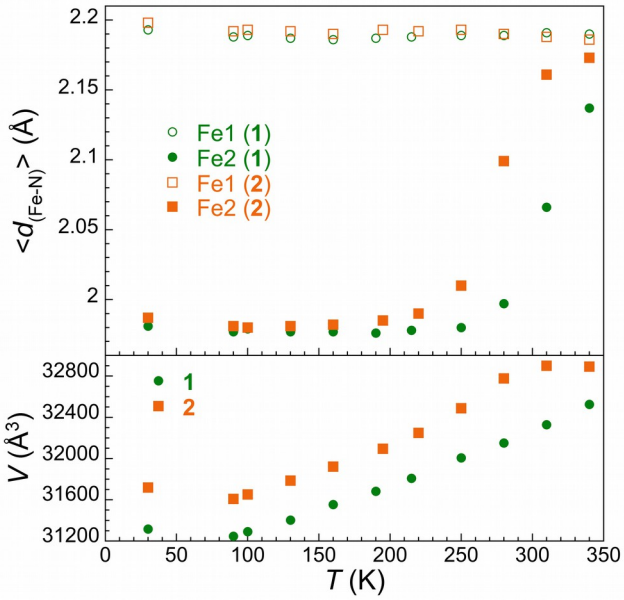

the space used by the ambient H_2O molecules to diffuse inside the crystal and occupy the space left by the MeOH species leaving the structure upon formation of **1a** while maintaining the crystallinity. The evacuation of guest MeOH molecules occurs probably through these layers as well.

Figure 2. Representation of a central $[Fe_2(H_2L)_3]^{4+}$ helicate (blue) of (1) and the surrounding five, equivalent, first neighbours (light green), emphasizing the π–π interactions formed by the latter. The C–H··· π interactions are not shown.

The asymmetric structure of **1** causes its Fe(II) centers to be in two different spin states at 100 K. A variable temperature crystallographic study was performed in order to visualize the thermal evolution of the magnetic states of both distinct Fe centers in this molecular assembly. Thus, full structure determinations were conducted for **1** at 30, 90, 100, 130, 160, 190, 215, 250, 280, 310 and 340 K (Table S1). It is interesting to note that as low as 30 K, Fe1 continues to be in the HS state ($<d_{(Fe-N)}>$ = 2.19 and 1.98 Å for Fe1 and Fe2) whereas at 340 K, Fe2 has switched almost entirely to the HS state ($<d_{(Fe-N)}>$ = 2.19 and 2.14 Å for Fe1 and Fe2). The evolution of $<d_{(Fe-N)}>$, with the temperature (Fig. 2) beautifully indicates a gradual SCO from near 250 K, consistent with bulk magnetic susceptibility measurements (see below). Interestingly, plots of cell parameters *vs* temperature do not mirror the SCO and only exhibit the expected thermal expansion associated to the temperature increase (Figs. 3 and S4). This indicates that the crystal lattice is capable of accommodating the structural changes associated with the ST without experiencing changes to the overall dimensions, which is in line with the observed gradual SCO (see below).

$Br@[Fe_2(H_2L)_3]Br(PF_6)_2\cdot 4CH_3OH$ (2). This compound (Tables S2 and S7) is isostructural with **2**, now involving Br^- ions instead of Cl^-, therefore, only the small differences will be highlighted here. The asymmetric unit also differs on the number of solvate molecules, here with four solvent MeOH molecules present. The structural and electronic dissimilarity between the Fe atoms (Fig. S5) of the assembly is here slightly less pronounced than in **1** (Tables 2 and S11) while still causing a different magnetic behavior. The metals at 100 K are thus in the HS ($<d_{(Fe-N)}>$ = 2.193 Å) and LS ($<d_{(Fe-N)}>$ = 1.980 Å), respectively. The variable temperature structural study of **2** (Table S2) shows that the gradual SCO of Fe1 is now shifted approximately 40 K towards lower temperatures, as is the evolution of the cell parameters (Figs. 3 and S4). In this evolution, a change of tendency is seen at 280 K and above probably related to the onset of MeOH extrusion.

Figure 3. Temperature dependence of the average Fe–N distances (top) and of the cell volume (bottom) for compounds **1** and **2** as determined through single crystal X-ray diffraction.

$Cl@[Fe_2(H_2L)_3]Cl(PF_6)_2\cdot 3CH_3OH\cdot H_2O$ (1a). Compound **1a** is organized in the tetragonal space group $I4_1acd$ (Tables S3 and S8) and incorporates sixteen asymmetric units into the unit cell. The composition of the asymmetric unit of **1a** differs from that of **1** in that 2.7 molecules of MeOH have now been replaced by one molecule of H_2O. The latter and one molecule of MeOH are disordered over two positions. The exchange of MeOH by H_2O, which occurs in a SCSC manner, leads to other important changes. The $(Cl@[Fe_2(H_2L)_3])^{3+}$ assembly becomes symmetric by virtue of a binary axis, thus the encapsulated Cl^- ion is located at the center of the host helicate at the same distances from both Fe atoms, now crystallographically equivalent (Tables 2 and S8). The increased symmetry is achieved because the external Cl^- ion is now disordered over two equivalent positions, near either one or the other Fe center (Fig. S6). This disorder shows that the exchange of guest molecules causes important relocations of atoms (besides these from the migrating species). Thus 50% of the Cl^- ions have experienced, either a displacement of approximately 9 Å (Fig. S7) or a partial substitution with the encapsulated anion in going *through* the helicate, from one side to the other. The crystallographic equivalence of the Fe ions in the lattice results from the averaging of all the disordered components, thus, is not mirrored by an equivalence of both atoms within individual molecules, which are clearly different (each external Cl^- ion can lie close to only one of both Fe centers at a time). This translates into a slightly different magnetic behavior for each metal (see below) that cannot however be put into evidence crystallographically, contrary to the case of **1**. Here both Fe centers are not so different from each other because the distribution of N−H···Cl^- *vs* N−H···O interactions (Tables 2 and S11) near one or the other metal is more even (Fig. S6) than in **1**. Thus, each molecule shows only three N−H···O interactions distributed near both Fe centers. The difference between Fe1 and Fe2 would be then much smaller than in compound **1**. Consistent with the observed magnetic properties (see below), at 90 K both Fe centers in **1a** show $<d_{(Fe-N)}>$ values proper of the LS state (1.983 Å). The structure of **1a** was determined at several temperatures; 30, 90, 215, 296 and 300 K. Inspection of the crystallographic parameters reveal that the metals are LS below 100 K ($<d_{(Fe-N)}>$ = 1.982, 1,983 Å at 30 and 90 K), and experience SCO upon warming to near completion at 300 K ($<d_{(Fe-N)}>$ = 2.048, 2.158 and 2.157 Å at 215, 296 and 300 K,

respectively). Both metals of the helicate remain structurally equivalent at all temperatures, therefore, the data available does not allow a description of the LS/HS states distribution among the metals during the transition. The organization of the system in the lattice is similar to that seen in **1** (Figs. 2 and S3), with the $(Cl@[Fe_2(H_2L)_3])^{3+}$ fragments disposed in sheets perpendicular to the *c* axis and connected through π···π and C–H···π interactions.

$Br@[Fe_2(H_2L)_3]Br(PF_6)_2\cdot MeOH\cdot H_2O$ (2a). Compound **2a** (Tables S4 and S9) is isostructural with **1a**, changing the Cl^- ions by Br^-, and only the differences with the latter are emphasized here. The solvent molecules of the asymmetric unit in **2a** are one molecule of MeOH and one diffuse molecule of H_2O. The distribution of counterions and solvate species here is more complex that for all the previous compounds. Thus, besides the diffused molecule of water, the molecule of MeOH is disordered over two positions. In addition, here the external Br^- is disordered over three positions (Fig. S8; Br2, Br3A and Br3B), which themselves are replicated by symmetry over three other equivalent locations. Br3A and Br3B share their space with a disordered PF_6^-, which occupies the void left in their absence. Thus, the guest exchange producing the **2** → **2a** transformation leads here to even more noticeable movements of atoms, including displacements of voluminous Br^- anions and PF_6^- species. This is particularly remarkable considering that the transformation takes place with preservation of the single crystal integrity. In studying processes **1** → **1a** and **2** → **2a**, it appears as if the largest contribution to the stability of the crystal lattice comes from the intermolecular interactions between the $(X@[Fe_2(H_2L)_3])^{3+}$ entities (Figs. S3 and 2), which is the same in the four compounds and provides a framework with enough space and flexibility for the movement of guest molecules through it. The crystallographic non-equivalence of the Fe centres in **2a** is not very pronounced, as reflected in the magnetic properties (see below). In fact, each molecule exhibits only one N−H···O contact, and it is rather weak, thus, not contributing significantly to the difference between both metal centers. At 90 K, the value of $<d_{(Fe\text{-}N)}>$ (2.000 Å) reflects a nearly complete LS spin state evidenced in the magnetic measurements (see below). The variable temperature structural determinations reflect the SCO behavior evidenced during magnetization studies with $<d_{(Fe\text{-}N)}>$ values of 1.997 Å at 30 K (LS), 2.116 Å at 215 K (~70% HS) and 2.177 Å at 296 K (HS).

$Cl@[Fe_2(H_2L)_3](I_3)_3\cdot 3Et_2O$ (1b). This compound crystallizes in the trigonal space group $R\bar{3}$ (Tables S5 and S10). The asymmetric unit corresponds to one third of the empirical formula while the unit cell encloses six times this formula. The main component of **1b** is a $(Cl@[Fe_2(H_2L)_3])^{3+}$ helical unit (Fig. 4) very similar to that seen in **1** and **1a**, present in the lattice as a racemic mixture of both possible enantiomers. The encapsulated Cl^- features also varying N–H···Cl^- interactions (Tables 2 and S11) rendering the two metal ions of the helicate inequivalent.

Figure 4. Side (A) and down the axis (B) views of the assembly $(Cl@[Fe_2(H_2L)_3](I_3)_3$ from **1b**, and the six molecules of Et_2O surrounding central helicate. The H_2L ligands are in three different colours (green, black and yellow), the remaining C atoms are grey, O is red, I is purple. Only crystallographically unique Fe, Cl and N atoms are labelled. Only hydrogen atoms on N atoms are shown (white).

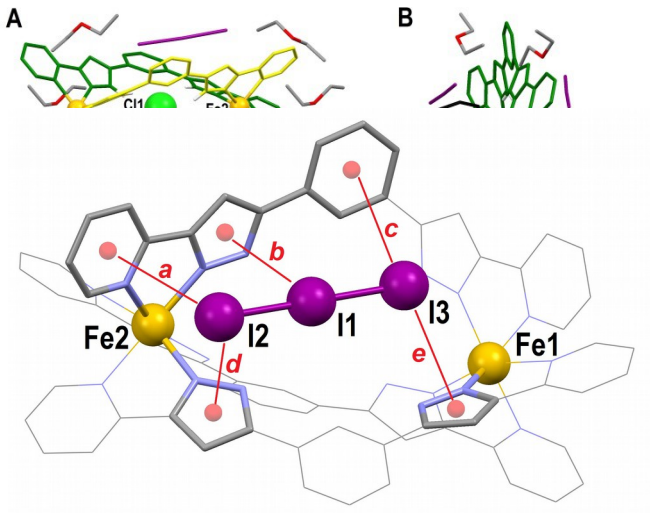

In this compound, the positive charges of the supramolecular assembly are compensated by three I_3^- linear anions, disposed along the sides of the helicate, approximately within the crevices left by the three ligand strands (Fig. S9) in a manner that also contributes to the difference in environments of both Fe centres. Here however, all the N–H groups are engaged in hydrogen bonding interactions only with the central Cl^- ion. Thus, consistent with the observations in **1**, **1a**, **2** and **2a**, both Fe centres of **1b**, lie now in the HS state for the whole range of temperatures (see below). This is reflected in the $<d_{(Fe\text{-}N)}>$ values observed at 100 K (of 2.185 and 2.188 Å for Fe1 and Fe2, respectively). Thus, in this compound, the crystallographic differences between both Fe centres do not reflect on disparate magnetic properties. The interaction of the I_3^- ions with the $(Cl@[Fe_2(H_2L)_3])^{3+}$ fragment of **1b** occurs *via* a succession of "lone pair – π" interactions with various aromatic rings from the H_2L ligands. In fact, a total of six contacts fulfil the criteria to consider such interaction[36] (Fig. 5), in a rare example where the three atoms of the anion interact with one or more aromatic rings. These interactions keep the central phenylene spacer and the concerned pyrazolylpyridine group of H_2L almost within the same plane (mutual angle of 10.3º) whereas the other pyrazolylpyridine moiety is twisted by 29.96º with respect to the central phenylene. Each $(Cl@[Fe_2(H_2L)_3])^{3+}$ assembly is surrounded also by six first neighbouring molecules of Et_2O (Fig. 4). Thus, the organization of this compound in the lattice does not produce alternating layers of respective hydrophilic and hydrophobic character as in **1** and **2**. Instead, the helical ensembles of **3** are disposed as infinite rods running along their axial direction, parallel to the crystallographic *c* axis (Fig. S10) and mutually shifted. Within the rods, pairs of enantiomeric $(Cl@[Fe_2(H_2L)_3])^{3+}$ groups are interlocked pairwise face to face, connected through six complementary and identical C–H···π contacts (Fig. S11). The mutual shift between rods cause each helicate to be surrounded laterally by six other equivalent neighbours connected to it by pairs of π···π interactions (Fig. S12).

Figure 5. Representation of the $[Fe_2(H_2L)_3]^{4+}$ moiety of **2b** (**1b** is analogous), emphasizing as red lines its "lone pair – π" interactions with one of the I_3^- groups. Centroid to atoms distances (Å) in the **1b**/**2b** format; 4.012/3.999 (a), 3.939/3.971 (b), 4.148/3.151 (c), 3.956/3.954 (e), 3.978/ (d).

Br@[Fe$_2$(H$_2$L)$_3$](I$_3$)$_3$·3Et$_2$O (2b). Compound **2b** is isostructural with **1b**, with the only significant difference that the anion encapsulated is now a Br^- species instead of Cl^-. This does not lead to significant differences to the lattice organization (Table S5, Figs. 4, 5 and S9 to S12), or to the metric parameters (Tables 2, S10, S11 and caption of Fig 5), thus, the description made for the Cl^- analogue is valid for the Br^- derivative. In addition, the Fe centers exhibit the same spin state as in **1b**, *ie* HS as observed crystallographically at 100 K (<$d_{(Fe-N)}$> = 2.185 and 2.189 Å for Fe1 and Fe2) and from variable temperature magnetic measurements (see below).

Encapsulating ability of the [Fe$_2$(H$_2$L)$_3$]$^{4+}$ host. The above structural studies show that the host helicate [Fe$_2$(H$_2$L)$_3$]$^{4+}$ is capable of encapsulating Cl^- or Br^-, while not being able of hosting I^- in its central cavity. Indeed, all attempts to prepare a hypothetical (I@[Fe$_2$(H$_2$L)$_3$])$^{3+}$ species failed, eventually even leading to the new product Cl@[Fe$_2$(H$_2$L)$_3$](I$_3$)$_3$·3Et$_2$O (**1b**), resulting from the presence of Cl^- traces in the system. The so-called packing coefficient, *PC*, has been previously employed to evaluate the possibility of encapsulating guests within a host cavity and its efficiency.[37] The *PC* of a host/guest system is the ratio of the volume of the guest over that of the host cavity ($PC=V_{guest}/V_{cav}$). The ideal *PC* for the case of encapsulation of liquids was shown to be 0.55 ± 0.09.[37] Higher values (0.60 – 0.79) have been found with host/guest systems involving strong intermolecular interactions.[38] The volume of the cavity inside the [Fe$_2$(H$_2$L4)$_3$]$^{4+}$ host was calculated from the molecular structure of compounds **1** and **2** as 28 and 33 Å^3, respectively, using Swiss-Pdb Viewer 4.1 (Fig. S13). The difference suggests that this host has a certain degree of flexibility and is capable to adjust its size depending on the nature of the guest. On the other hand, the volume of halide ions was calculated from their ionic radii as 19.51, 25.52 and 36.62 Å^3, for Cl^-, Br^- and I^-, respectively.[39] The calculated *PC* values for Cl^- and Br^- in **1** and **2** are 0.697 and 0.773, respectively. These higher than the ideal value (0.55) numbers are expected, considering the strong N–H···X$^-$ H-bonding interactions involved in these host/guest systems. In addition, it is possible that for the case of monoatomic anions (such as halides) the ideal *PC* value is larger than for liquids. For the case of I^-, it appears indeed that the volume of the anion seems excessive to accommodate within this host.

Thermal Spin Crossover Properties

The extensive crystallographic studies on the supramolecular assemblies **1**, **1a**, **1b**, **2**, **2a** and **2b**, revealed a fascinating variety of magnetic states and STs that were investigated in detail by means of bulk magnetic and calorimetric measurements.

Magnetic susceptibility data were collected on microcrystalline samples of all compounds described above, under a constant magnetic field of 0.5 T, from 1.9 to either 350 or 380 K. The results are represented on Figs. 6 and S14 in form of χT *vs* *T* plots. For compound **1**, the value of χT at 380 K is 7.15 cm^{3}Kmol^{-1}, which shows that both Fe(II) ions of the supramolecular helicate are in the HS state ([HS–HS], $S = 2$, $g = 2.38$), as also indicated by the single crystal X-ray diffraction experiments (see above). A clear decline is observed

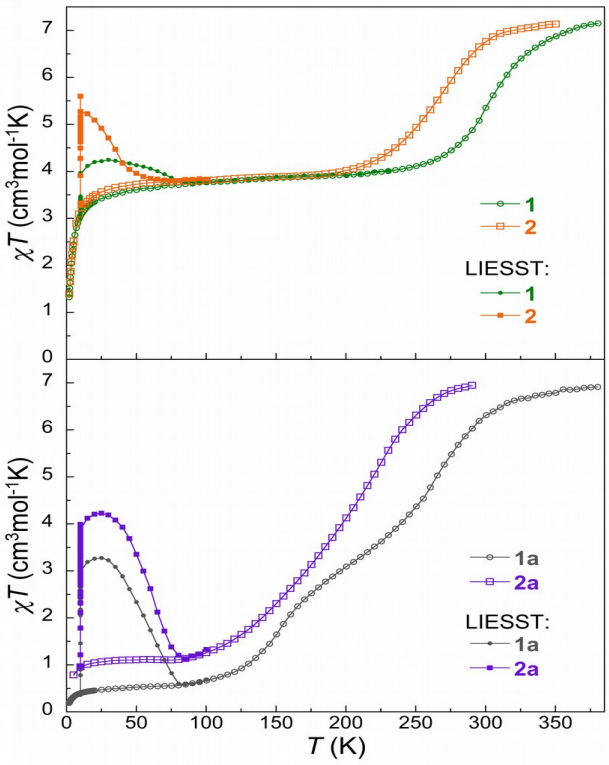

immediately upon cooling, reaching a plateau near 250 K, at 3.9-3.7 cm^{3}Kmol^{-1} down to 50 K, showing that half of the Fe(II) centers of the system experience an almost complete SCO, centered near room temperature ($T_{1/2}$ = 305 K). This is consistent with the crystallographic data at 100 K, which shows that each of the two crystallographically distinct Fe centers of the helicate of **1** is at this temperature in a different spin state ([LS–HS]). Near 25 K, the χT curve exhibits a new sharp decline that is attributed to the zero field splitting (ZFS) effect of the remaining HS metal centers. The Br^- analogue (compound **2**) exhibits an almost identical behavior to **1**, with the only difference that the SCO is shifted 40 K to lower temperatures ($T_{1/2}$ = 265 K).

The above observations are mirrored by broad anomalies observed at the corresponding temperatures in the $C_p(T)$ curves (Fig. S15, C_p is the molar heat capacity at constant pressure), and thus ascribed to the SCO processes of compounds **1** and **2**. From the excess heat capacity associated with these, obtained by subtracting the estimated lattice contribution (Fig. 7), the excess enthalpy ΔH_{SCO} and entropy ΔS_{SCO} due to the SCO are determined to be 4.79/3.85 kJmol^{-1} and 15.95/15.01 Jmol^{-1}K^{-1}, respectively, for **1**/**2**. In both compounds, the excess entropy is only slightly higher than the purely electronic component of the ST of one Fe(II) center, *R*ln5, indicating a very weak coupling of the SCO with lattice phonons, in agreement with the gradual nature of the transition. A more quantitative measure of the cooperative character of the SCO is derived by modeling the excess heat capacity with Sorai's model, that considers domains with interacting *n* like-spin centers.[40-41] Here, the data for **1**/**2** are nicely reproduced with T_{SCO} = 302.1(3)/258.2(3) K and n = 15.8(5)/14.6(4) (Fig. 7). The derived T_{SCO} values are in excellent agreement with the magnetic susceptibility data, while the values of n are intermediate between weekly cooperative SCO compounds[42-43] and highly cooperative ones.[44-45]

Figure 6. Temperature dependence of χT (empty symbols as indicated) for **1**, **2** (top), **1a** and **2a** (bottom). Full symbols depict in all cases the increase upon irradiation with green light at 10 K corresponding to the LIESST effect, as well as the relaxation back to the LS ground state upon warming (see text).

Figure 7. Excess heat capacities associated with the SCO in **1**, **2** and **1a**, as indicated. The full black lines are fits to Sorai's domain model for respectively T_{SCO} = 302.1 and n = 15.8, T_{SCO} = 258.2 K and n = 14.6, and T_{SCO} = 185.0/258.9 and n = 7.1/15.5.

The only chemical difference between compounds **1** and **2** is the nature of the encapsulated and external X^- ions (Cl^- *vs* Br^-), which influence the crystal field around Fe1 *via* N–H···X^- hydrogen bonds. The presence of Cl^- stabilizes the LS state with respect to Br^-, in contradiction with previous observations made for other SCO systems exhibiting similar N–H···X^- out-of-coordination sphere interactions.[34] The discrepancy could be due to the fact that in the current systems the N–H groups are in α with respect to the Fe–N bonds, whereas in the reported compounds the N–H functionalities are two bonds away from the Fe–N moieties.

The dramatic effect caused by the SCSC **1** → **1a** transformation on the magnetic properties of the $(Cl@[Fe_2(H_2L)_3])^{3+}$ species could be quantified through susceptibility measurements. Thus, at 380 K, the χT product of **1a** amounts to 7.15 cm^{3}Kmol^{-1}, showing both Fe centers of the assembly to lay in the HS state (g = 2.38). Upon cooling, a SCO of 50% of the Fe centers is also observed, at a temperature slightly lower ($T_{1/2}$ = 265 K) than the parent compound **1**. Upon further cooling a second ST process initiates that is almost complete near 100 K, leading thus to the [LS–LS] configuration, with $T_{1/2}$ = 160 K. Therefore, in consistency with the structural analysis, both Fe centers of each individual molecule are not equivalent, which translates into a two-step SCO arising from the slightly different magnetic behavior of each metal site in the helicate. On the contrary, compound **2a** shows a gradual nearly complete SCO (~85% completion) with $T_{1/2} \approx$ 200 K in one unique step covering almost 200 K. This is consistent with the crystal structure, which shows almost no difference between Fe1 and Fe2 in terms of out-of-coordination sphere contacts (see above).

Calorimetry studies support these observations. First, two consecutive anomalies associated with two SCO steps are clearly distinguished for **1a** (Fig. S15). Indeed, the corresponding excess heat capacity is nicely reproduced by the domain model using two transitions with T_{SCO} = 185.0(3)/258.9(3) K and n = 7.1(3)/15.5(1) (Fig. 7), thus in excellent agreement with the magnetic data. The lower temperature step is thus markedly less cooperative, with a domain size n about half that for the higher temperature step or these for the SCO in **1** and **2**. The total excess enthalpy ΔH_{SCO} and entropy ΔS_{SCO} amount to 6.03 kJmol^{-1} and 26.60 Jmol^{-1}K^{-1}, characteristic of a weakly-cooperative system, involving a very weak coupling of the SCO with lattice phonons. On the other hand, the $C_p(T)$ of compound **2a** hardly exhibits any anomaly, as a consequence of the extremely gradual and broad nature of the SCO process, in addition to the fact that it occurs down to the lowest temperature accessible with the DSC set-up, 100 K.

Compounds **1b** and **2b** exhibit χT values near 7.7 and 7.5 cm^{3}Kmol^{-1}, respectively, in most of the studied temperature range, until a sudden decrease occurs below near 50 K (Fig. S14). The large plateau shows that the Fe(II) sites in both compounds are in the [HS-HS] state and do not experience any SCO. The spin projections of the S = 2 spin state of these ions are subject to ZFS, which causes the deviation from the Curie-Law at the lowest temperatures, in a similar manner as for the [LS-HS] state in compounds **1** and **2**.

Overall, the combined crystallographic and magneto-thermal

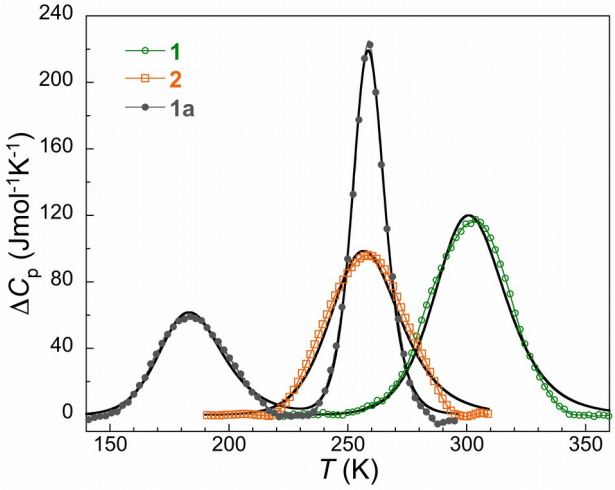

data demonstrate that temperature, chemical reagents and guest solvent molecules allow to access and characterize three different magnetic states of the $(X@[Fe_2(H_2L)_3])^{3+}$ assembly (X=Cl, Br), while the temperature of the transitions may be shifted by 40 K with the nature of the ion X^-. Each of the three possible states may be reached and maintained for large ranges of temperatures, namely [HS–HS] (over more than 400K; **1b** and **2b**), [LS–HS] (over more than 200K; **1**) and [LS–LS] (over more than 100K; **1a**). **While the versatility of this system is remarkable, the occurrence of [HS–LS] situations is not new.[46] It has been identified in several instances before,**

sometimes involving helicates[22] or in several other discrete dinuclear complexes.[47-49] However, this well-defined spin mixing is not limited to [Fe$_2$] molecules. It can be found in mononuclear systems,[50-51] in clusters of other nuclearities[14, 52-53] or in coordination polymers.[54-55]

Light induced transitions.

The possibility of employing an additional means of manipulating the magnetic state of the Fe centers at low temperature in the present $(X@[Fe_2(H_2L)_3])^{3+}$ helicates by exploiting the LIESST effect[56] was investigated. Compounds **1/2** were brought to their [LS–HS] state by cooling them to 10 K and were then irradiated with light in the wavelength range of 500-650 nm. This caused a sudden increase of the χT value, reaching quasi saturation after <1000 *s* at 3.9/5.6 cm^3Kmol^{-1} (Figs. 6 and S16). Considering that at this temperature the effect of Fe(II) ZFS is already very apparent, the jump in susceptibility in the case of **2** corresponds to a [LS–HS] → [HS–HS] transformation of the system of nearly 100% of the molecules, which reach in this manner a trapped metastable [HS-HS] state. Given that samples of very small and similar thickness were used in this study, the effect of light propagation should be minor. Therefore the incomplete transition in **1** can mostly be associated with the SCO occurring at higher temperatures.[57] Another contribution may also result from competition with the relaxation back to the [LS-HS] state, which appears to be slow, but active already at 10 K. Indeed, upon increasing the temperature, a decrease of the χT sets in almost immediately caused by the relaxation to the [LS–HS] state, which is completed at 80/75 K. As a consequence, a ~~The process occurs with an ill-defined but low~~ characteristic T_{LIESST} can not be determined with confidence, although it is clearly rather low.[58]

Irradiation of compounds **1a**/**2a** at 10 K, lying in their stable [LS–LS] state, using the same quality of light, also causes a sudden increase of the χT product, reaching saturation at values of 3.1/4.0 cm^3Kmol^{-1} after <2000 s (Figs. 6 and S16). Taking again into account the significant ZFS of the HS metastable state, these values point at a transformation from the LS to the HS state of at least 50% of the Fe centers of the sample. In the case that each metal of the molecule exhibits a different behavior, this would correspond to a 100% [LS–LS] → [LS–HS] transformation, possibly in addition to partial transformation to the [HS–HS] state. The aforementioned non-equivalence is plausible for **1a** since the susceptibility measurements have served to demonstrate that there are two slightly magnetically different metals in this compound. The slight asymmetry would also be consistent with the interpretation of crystallographic data in both compounds. Upon increasing the temperature after turning off the light, both compounds exhibit a very similar behaviour, with the relaxation of the induced metastable state to the [LS–LS] state only occurring above *ca.* 25 K, with the same characteristic T_{LIESST} of *ca.* 60 K. Such similarity would support that the excitation of **2a** also corresponds to a full [LS–LS] → [LS–HS] transition. It may appear surprising that the light-induced transformation in **1a** and **2a** seems to be limited to the [LS–LS] → [LS–HS] transition, given that the further [LS–HS] → [HS–HS] transformation is indeed observed, on irradiation, in the parent compounds **1** and **2**. It could be that the [LS-HS] configuration is stabilized once formed in **1a** and **2a**.

These experiments demonstrate another mechanism of accessing the [LS–HS] or [HS–HS] states of the $(X@[Fe_2(H_2L)_3])^{3+}$ unit by means of an external stimulus.

Stability in Solution

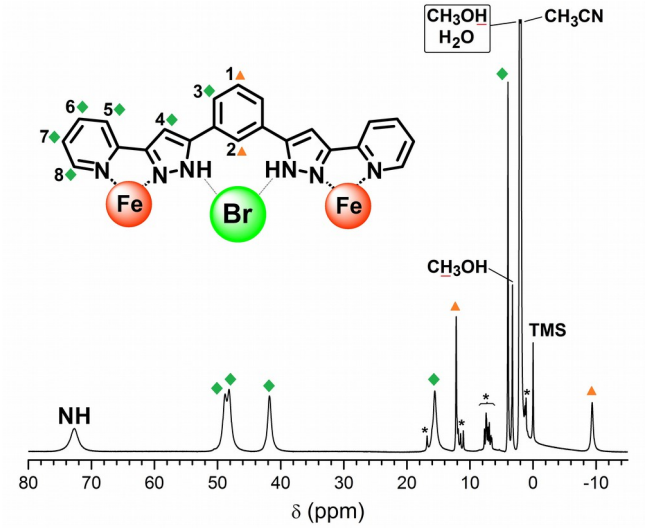

The stability of the $(X@[Fe_2(H_2L)_3])^{3+}$ assembly in solution was investigated by means of ^{1}H NMR and mass spectrometry. Such studies are dependent on the solubility of the compounds. DMSO was found to dissolve all complexes, however, it was established by NMR that the assemblies decompose in this medium. Compounds **1b** and **2b** are not soluble in any other common solvents, while MeCN is one of the few media where **1** and **2** can be dissolved. In this solvent, complex **1** exhibits a dominant set of nine broad, paramagnetically shifted peaks (between –6 and 60 ppm) with no hyperfine splitting of which, two integrate for half the intensity of the other seven (Fig S17). Two of the latter resonances are degenerate near 40 ppm, but comparison with the Br^- analogue (see below) unveils the existence of two peaks in that area. These features are consistent with the idealized symmetry shown by the helicate of **1** in the solid state (D_3), suggesting that this is the major species in solution. The spectrum shows a smaller set of broad signals, spanning over a narrower range of chemical shifts (1 to 15 ppm). Their compared integrations are consistent with the ensemble arising from a multiple of sixteen protons (Fig S18). This is in agreement with a coordination complex with all identical H_2L ligands but featuring lower symmetry than the helical assembly. In fact one species exhibiting H_2L coordinated to only one Fe(II) with formula $[Fe(H_2L)_3]^{2+}$ can be isolated and characterized from this reaction system, which would explain this response.[59] Under this premise, comparison of total integration values indicates that the helicate in **1** and the mononuclear complex coexist in approximately 1:0.6 proportions. The ^{1}H NMR spectrum of **2** (Fig. 8) corroborates the observations made with its Cl^- analogue. The main differences are *i*) the set of peaks for the minor species is now much weaker (indicating now an approximate partition of 1:0.1, Fig. S19), *ii*) the signal that was degenerate in **1** is now resolved in two peaks, *iii*) a resonance that in **1** was located in between the signals of residual MeOH has now moved under one of the solvent peaks, *iv*) the most

paramagnetically shifted peaks of the helicate exhibit now significantly larger chemical shifts. This experiment confirms that the $(Br@[Fe_2(H_2L)_3])^{3+}$ unit is stable in MeCN with clear dominance over the less symmetric species and that **2** in solution exhibits a larger fragment of Fe(II) centers in the HS state than **1** (consistent with the solid state behaviour) as indicated by much larger paramagnetic shifts.

Positive electron spray ionization mass spectrometry (ESI^+-MS) experiments were also performed for **1** and **2** in MeCN. The results for **1** confirm the existence of the helicate assembly in solution with identification of the fragments $(Cl@[Fe_2(H_2L)_2(HL)])^{2+}$ at m/z = 619.13 and $[Fe_2(H_2L)(HL)_2]^{2+}$ at m/z = 601.15 (Fig. S20). The presence of the latter may reflect an equilibrium between the occupied and vacant host. In addition, peaks reflecting assemblies of the lower symmetry species[59] were also evident (associated as dimers, such as $[Fe_2(H_2L)_5(HL)Cl]^{2+}$, m/z = 1165.86; $[Fe_2(H_2L)_6Cl(PF_6)]^{2+}$, m/z = 1239.36; $[Fe_2(H_2L)_4(HL)_2]^{2+}$, m/z = 1147.37). Interestingly, no signals linked to any coordination complex were detected for **2**. It is plausible that the $(Br@[Fe_2(H_2L)_2(HL)])^{2+}$ assembly is not amenable to travelling appropriately under the experimental set up. The absence of any other "non-halogen" species, which otherwise appear in the MS of **1**, is consistent with their very low presence in solutions of **2**, as suggested by NMR spectroscopy.

Figure 8. ^{1}H NMR spectrum of **2** in d_3-MeCN at room temperature, evidencing the stability of the $(Br@[Fe_2(H_2L)_3])^{3+}$ in solution. One of the protons labelled as a green rhombus is thought to lie under the solvent signals (see text). The asterisks correspond to a very minor species with lower symmetry (see text).

Conclusions

Existing concepts from supramolecular chemistry have been borrowed through the design and preparation of the dinucleating ligand H_2L, for the preparation of the functional host-guest helical architecture $(X@[Fe_2(H_2L)_3])^{3+}$ (X= Cl^-, Br^-). The nature of the guest, of the counter anions and of the accompanying solvate molecules in the crystal lattice are varied by selection of the synthetic protocol or by letting some of the obtained solids evolve in contact with the atmosphere, always leading to compounds amenable to SCXRD analysis. This has unveiled the possibility of accessing at will the three possible magnetic states of the assembly, [LS–LS], [LS–HS] and [HS–HS], over large temperature ranges, using various different pathways, as corroborated in detail *via* magnetic studies. The thermodynamic features of these transformations have been described through calorimetry. The use of light as external stimulus represents an additional mechanism of undergoing the [LS–LS] → [LS–HS] and [LS–HS] → [HS–HS] transitions. Solution studies demonstrate that the helical assemblies are maintained in certain solvents. This study illustrates the great potential that the confluence of coordination supramolecular chemistry with the exploitation of the switching properties of transition metals may have for the development of functional nanoscopic devices.

Experimental Section

Synthesis

1,3-*bis*-(1-oxo-3-(pyridine-2-yl)-propionyl)-benzene, H_2L1. To a suspension of 60% NaH oil dispersion (2g, 50 mmol) in 150 ml THF was added 1,3-diacetylbenzene (2g, 12.3 mmol) and the mixture was stirred for 15 minutes. Then 2-ethylpicolinate (3.4 ml, 24.7 mmol) in 50 ml THF was added dropwise, and the mixture brought and left to reflux overnight. A green-mustard suspension was formed after that, which was quenched with 5 ml EtOH and the resulting solid was then collected by filtration. The solid was suspended in 150 ml H_2O, the pH was adjusted to 2-3 using 12% HCl and the mixture was left 30 minutes under stirring. The yellow solid was collected by filtration, washed with water and dried under vacuum. The yield was 3.4 g (73.8 %). ^{1}H NMR in $CDCl_3$, δ (ppm): 7.43 (*m*, 2H); 7.56 (*m*, 2H); 7.66 (*s*, 2H); 7.86 (*t*, 2H); 8.16 (*d*, 2H); 8.21 (*dd*, 2H); 8.69 (*m*, 2H); 16.45 (broad *s*, 2H). m/z = 373.12 $(M+H)^+$.

1,3-*bis*-(1-(pyridine-2-yl)-pyrazol-3-yl)-benzene, H_2L. Solid H_2L1 (1.5 g, 4 mmol) was suspended in $CHCl_3$ (100 ml) and 20% excess hydrazine (64% in H_2O, 0.73 ml, 9.6 mmol) was added to the mixture dropwise, which was then brough to reflux and maintained like that overnight. After that, the mixture is cooled to room temperature and the solvents were removed by rotary evaporation. An oily residue formed which was suspended in water and stirred for about an hour. A white solid was collected by filtration, washed with ether and dried under vacuum. The yield was 0.77 g (52 %). ^{1}H NMR in DMSO, δ (ppm): 7.32 (*t*, 2H); 7.46 (*s*, 2H); 7.54 (*t*, 1H); 7.90 (*m*, 6H); 8.40 (*s*, 1H); 8.63 (*s*, 2H); 13.52 (very broad, NH groups). *Anal.* Calc. (Found) for **H_2L**·0.5H_2O: C, 70.76 (70.39); H, 4.59 (4.37); N, 22.51 (22.48). m/z = 365.17 $(M+H)^+$.

$Cl@[Fe_2(H_2L)_3]Cl(PF_6)_2$·5.7$CH_3OH$ (1). A suspension of H_2L (25 mg, 0.069 mmol) in methanol (10 mL) was added dropwise to a methanolic solution (5 mL) of $FeCl_2$.4H_2O (9.1 mg, 0.046 mmol). A red solution formed, which was stirred for 45 minutes, filtered and the filtrate mixed with a methanolic (2 mL) solution of NBu_4PF_6 (14 mg, 0.036 mmol). The resulting solution was layered with ether, which yielded red crystals after a few days. The yield was 17 mg (42%). *Anal.* Calc. (Found) for **1**: C, 49.25 (49.18); H, 4.08 (4.24); N, 14.42 (14.30).

$Cl@[Fe_2(H_2L)_3]Cl(PF_6)_2$·3$CH_3OH$·$H_2O$ (1a). Crystals of **1** were isolated by filtration and placed on a clean filter paper in the air for 5 days. The aged crystals, now of **1a**, were still suitable for single crystal X-ray diffraction. *Anal.* Calc. (Found) for **1a**: C, 48.81 (49.18); H, 3.80 (4.24); N, 14.85 (14.31).

$Br@[Fe_2(H_2L)_3]Br(PF_6)_2$·4$CH_3OH$ (2). A suspension of H_2L (25 mg, 0.069 mmol) in methanol (10 mL) was added dropwise to a methanolic solution (5 mL) of $FeBr_2$ (9.9 mg, 0.046 mmol). A red solution formed, which was stirred for 45 minutes, filtered and the filtrate mixed with a methanolic solution (2 mL) of NBu_4PF_6 (14 mg, 0.036 mmol). The resulting solution was layered with ether, which yielded red crystals after a few days. The yield was 17 mg (41%). *Anal.* Calc. (Found) for **2**·2H_2O: C, 46.22 (46.49); H, 3.76 (3.83); N, 13.86 (13.36).

$Br@[Fe_2(H_2L)_3]Cl$·$(PF_6)_2$·MeOH·H_2O (2a). Crystals of **2** were isolated by filtration and placed on a clean filter paper in the air for 5 days. The aged crystals, now of **2a**, were still suitable for single crystal X-ray diffraction. *Anal.* Calc. (Found) for **2a**: C, 45.43 (45.92); H, 3.49 (3.95); N, 14.23 (13.62).

$Cl@[Fe_2(H_2L)_3](I_3)_2$·3Et_2O (1b). A suspension of H_2L (25 mg, 0.069 mmol) in methanol (10 mL) was added dropwise to a methanolic solution (5 mL) of $FeCl_2$ (9.1 mg, 0.046 mmol). A red solution formed which was stirred for 30 minutes and filtered. The filtrate was mixed with a methanolic solution (15 mL) of NBu_4I (40 mg, 0.108 mmol) and the resulting solution was layered with ether, which yielded red crystals after ten days. The yield of crystals was The yield was 7 mg (12%). *Anal.* Calc. (Found) for **1b**·0.5Et_2O: C, 36.36 (36.68); H, 3.17 (2.80); N, 9.54 (9.88).

Br@[Fe$_2$(H$_2$L)$_3$](I$_3$)$_2$·3Et$_2$O (2b). A suspension of H$_2$L (25 mg, 0.069 mmol) in methanol (10 mL) was added dropwise to a methanolic solution (5 mL) of FeBr$_2$ (14.8 mg, 0.046 mmol). A red solution formed which was stirred for 30 minutes and filtered. The filtrate was mixed with a methanolic solution (15 mL) of NBu$_4$I (40 mg, 0.108 mmol) and the resulting solution was layered with ether, which yielded red crystals after ten days. The yield of crystals was 9 mg (14%). *Anal.* Calc. (Found) for **2b** (–2.5Et$_2$O): C, 33.14 (33.02); H, 2.16 (2.08); N, 10.23 (10.16).

X-ray crystallography

Data for compounds **1**, **2**, **1a** and **2a** were collected at various temperatures in the range 30-340 K on Beamline 11.3.1 at the Advanced Light Source, on a Bruker D8 diffractometer equipped with a PHOTON 100 CCD detector and using silicon 111 monochromated synchrotron radiation (= 0.7749 Å). The crystals were mounted on a MiTegen kapton loop and placed in the N_2 stream of an Oxford Cryosystems Cryostream Plus or for the lowest temperature (30 K) in the He stream from a Cryoindustries of America LT-HE Cool cryosystem. Data for compounds **1b** and **2b** were collected at 100 K on a Bruker APEXII QUAZAR diffractometer equipped with a microfocus multilayer monochromator with MoK radiation (= 0.71073Å).

Data reduction and absorption corrections were performed with SAINT and SADABS,[60] respectively. All structures were solved by intrinsic phasing with SHELXT[61] and refined by full-matrix least-squares on F^2 with SHELXL-2014.[61] All details can be found in CCDC 1455575-1455585 (**1**), 1455591-1455601 (**2**), 1455315-1455318 (**1a**), 1455319-1455322 (**2a**), 1455323 (**1b**) and 1455324 (**2b**), that contain the supplementary crystallographic data for this paper. These data can be obtained free of charge from The Cambridge Crystallographic Data Center via https://summary.ccdc.cam.ac.uk/structure-summary-form. Crystallographic and refinement parameters are summarized in Tables S1-S4. Selected bond lengths and angles and intermolecular distances are given in Tables 2 and S5-S11.

Physical Measurements

Variable-temperature magnetic susceptibility data were obtained with either MPMS5 or MPMS-XL SQUID magnetometers through the Physical Measurements unit of the Servicio de Apoyo a la Investigación-SAI, Universidad de Zaragoza. For the irradiation studies the commercial FOSH set-up was used in combination with a Xe arc lamp and short-pass and long-pass interference filters. The samples were in the form of small pieces of very thin pellets, to minimize the effect of the attenuation of the propagation of light through the sample. The data were corrected for the sample holder contributions, determined empirically as well as for the intrinsic diamagnetism of the samples, estimated using Pascal constants. Differential Scanning Calorimetry (DSC) measurements were done with a Q1000 calorimeter from TA Instruments equipped with the LNCS accessory, using aluminium pans crimped mechanically and an empty pan as reference. The temperature and enthalpy scales were calibrated with a standard sample of indium, using its melting transition (156.6 ºC, 3296 Jmol^{-1}). The zero-heat-flow procedure described by TA Instruments was followed to derive heat capacities, using a synthetic sapphire as reference compound. An overall accuracy of about 0.2 K and up to 10% was estimated respectively for the temperature and heat capacity over the whole temperature range. The lattice contributions to the heat capacity were estimated from the data above and below the observed anomalies. Excess enthalpy and entropy were derived by integration of the excess heat capacity with respect to T and ln$T$, respectively. Elemental analyses were performed with an Elemental Microanalizer (A5), model Flash 1112 at the Servei de Microanàlisi of CSIC, Barcelona, Spain. IR spectra were recorded as KBr pellet samples on a Nicolet AVATAR 330 FTIR spectrometer. Positive ion ESI TOF mass spectrometry experiments were performed on a LC/MSD-TOF (Agilent Technologies) at the Unitat d'Espectrometria de Masses de Caracterització Molecular (CCiT) of the University of Barcelona. The experimental parameters were: capillary voltage 4 kV, gas temperature 325ºC, nebulizing gas pressure 15 psi, drying gas flow 7.0 L min^{-1}, and fragmentor voltage ranging from 175 to 300 V. Samples (µL) were introduced into the source by a HPLC system (Agilent 1100), using a mixture of H$_2$O/MeCN (1/1) as eluent (200 µL min^{-1}).

Acknowledgements

GA thanks the Generalitat de Catalunya for the prize *ICREA Academia 2008* and *2013*, for excellence in research and the ERC for a Starting Grant (258060 FuncMolQIP). The authors thank the Spanish MICINN for funding through CTQ2012-32247 (GA, LAB), MAT2011-24284 (OR). MD thanks Avempace II Erasmus Mundus Action 2 program for a PhD scholarship. Data for compounds **1**, **2**, **1a** and **2a** were collected through access to ALS beamline 11.3.1. The Advanced Light Source is supported by the Director, Office of Science, Office of Basic Energy Sciences of the U. S. Department of Energy under contract no. DE-AC02-05CH11231.

Keywords: Spin Crossover • Fe(II) • Supramolecular Chemistry • Coordination Chemistry • Crystallography

[1] P. Gutlich, Y. Garcia, H. A. Goodwin, *Chem. Soc. Rev.* **2000**, *29*, 419-427.

[2] P. Gütlich, A. Hauser, H. Spiering, *Angew. Chem. Int. Ed.* **1994**, *33*, 2024-2054.

[3] P. Guionneau, *Dalton Trans.* **2014**, *43*, 382-393.

[4] M. A. Halcrow, *Chem. **Lett.** **2014**, **43**, **1178-1188.***

[5] H. J. Shepherd, T. Palamarciuc, P. Rosa, P. Guionneau, G. Molnar, J.-F. Letard, A. Bousseksou, *Angew. Chem. Int. Ed.* **2012**, *51*, 3910-3914.

[6] G. A. Craig, J. Sanchez Costa, O. Roubeau, S. J. Teat, H. J. Shepherd, M. Lopes, G. Molnar, A. Bousseksou, G. Aromi, *Dalton Trans.* **2014**, *43*, 729-737.

[7] A. Hauser, *Spin Crossover in Transition Metal Compounds II* **2004**, *234*, 155-198.

[8] M. Ohba, K. Yoneda, G. Agusti, M. C. Munoz, A. B. Gaspar, J. A. Real, M. Yamasaki, H. Ando, Y. Nakao, S. Sakaki, S. Kitagawa, *Angew.* Chem., Int. Ed.* **2009, *48*, 4767-4771.

[9] T. D. Roberts, F. Tuna, T. L. Malkin, C. A. Kilner, M. A. Halcrow, *Chem. Sci.* **2012**, *3*, 349-354.

[10] J. Sanchez Costa, S. Rodriguez-Jimenez, G. A. Craig, B. Barth, C. M. Beavers, S. J. Teat, G. Aromi, *J. Am. Chem. Soc.* **2014**, *136*, 3869-3874.

[11] G. Molnar, L. Salmon, W. Nicolazzi, F. Terki, A. Bousseksou, *J. Mater. Chem. C* **2014**, *2*, 1360-1366.

[12] Y. E. Alexeev, B. I. Kharisov, T. C. Hernandez Garcia, A. D. Garnovskii, *Coord. Chem. Rev.* **2010**, *254*, 794-831.

[13] L. Zhang, Y.-J. Lin, Z.-H. Li, G.-X. Jin, *J. Am. Chem. Soc.* **2015**, *137*, 13670-13678.

[14] T. Matsumoto, G. N. Newton, T. Shiga, S. Hayami, Y. Matsui, H. Okamoto, R. Kumai, Y. Murakami, H. Oshio, *Nat. Commun.* **2014**, *5*.

[15] C. Piguet, M. Borkovec, J. Hamacek, K. Zeckert, *Coord. Chem. Rev.* **2005**, *249*, 705-726.

[16] C. R. K. Glasson, L. F. Lindoy, G. V. Meehan, *Coord. Chem. Rev.* **2008**, *252*, 940-963.

[17] C. Piguet, C. Edder, S. Rigault, G. Bernardinelli, J.-C. G. Bunzli, G. Hopfgartner, *J. Chem. Soc., Dalton Trans.* **2000**, 3999-4006.

[18] F. Tuna, M. R. Lees, G. J. Clarkson, M. J. Hannon, *Chem., Eur. J.* **2004**, *10*, 5737-5750.

[19] L. J. Charbonnière, A. F. Williams, C. Piguet, G. Bernardinelli, E. Rivara-Minten, *Chem., Eur. J.* **1998**, *4*, 485-493.

[20] Y. Sunatsuki, R. Kawamoto, K. Fujita, H. Maruyama, T. Suzuki, H. Ishida, M. Kojima, S. Iijima, N. Matsumoto, *Inorg. Chem.* **2009**, *48*, 8784-8795.

[21] N. Struch, J. G. Brandenburg, G. Schnakenburg, N. Wagner, J. Beck, S. Grimme, A. Lützen, *Eur. J. Inorg. Chem.* **2015**, *2015*, 5503-5510.

[22] R. J. Archer, C. S. Hawes, G. N. L. Jameson, V. McKee, B. Moubaraki, N. F. Chilton, K. S. Murray, W. Schmitt, P. E. Kruger, *Dalton Trans.* **2011**, *40*, 12368-12373.

[23] D. Pelleteret, R. Clerac, C. Mathoniere, E. Harte, W. Schmitt, P. E. Kruger, *Chem. Commun.* **2009**, 221-223.

[24] S. Goetz, P. E. Kruger, *Dalton Trans.* **2006**, 1277-1284.

[25] F. Cui, S. Li, C. Jia, J. S. Mathieson, L. Cronin, X.-J. Yang, B. Wu, *Inorg. Chem.* **2012**, *51*, 179-187.

[26] J. Xu, T. N. Parac, K. N. Raymond, *Angew. Chem. Int. Ed.* **1999**, *38*, 2878-2882.

[27] C. R. K. Glasson, G. V. Meehan, C. A. Motti, J. K. Clegg, P. Turner, P. Jensen, L. F. Lindoy, *Dalton Trans.* **2011**, *40*, 12153-12159.

[28] R. A. Bilbeisi, S. Zarra, H. L. C. Feltham, G. N. L. Jameson, J. K. Clegg, S. Brooker, J. R. Nitschke, *Chem., Eur. J.* **2013**, *19*, 8058-8062.

[29] M. D. Ward, *Chem. Commun.* **2009**, 4487-4499.

[30] C. S. Hawes, C. M. Fitchett, P. E. Kruger, *Supramol. Chem.* **2012**, *24*, 553-562.

[31] G. Aromí, P. Gamez, J. Reedijk, *Coord. Chem. Rev.* **2008**, *252*, 964-989.

[32] M. Yamada, E. Fukumoto, M. Ooidemizu, N. Bréfuel, N. Matsumoto, S. Iijima, M. Kojima, N. Re, F. Dahan, J.-P. Tuchagues, *Inorg. Chem.* 2005, *44*, 6967-6974.

[33] G. A. Craig, J. S. Costa, O. Roubeau, S. J. Teat, G. Aromí, *Chem-Eur J* 2011, *17*, 3120-3127.

[34] G. Lemercier, N. Brefuel, S. Shova, J. A. Wolny, F. Dahan, M. Verelst, H. Paulsen, A. X. Trautwein, J.-P. Tuchagues, *Chem., Eur. J.* 2006, *12*, 7421-7432.

[35] S. A. Barrett, C. A. Kilner, M. A. Halcrow, *Dalton Trans.* **2011**, *40*, 12021-12024.

[36] T. J. Mooibroek, P. Gamez, *CrystEngComm* **2013**, *15*, 1802-1805.

[37] S. Mecozzi, J. J. Rebek, *Chem., Eur. J.* **1998**, *4*, 1016-1022.

[38] J. Rebek, *Acc. Chem. Res.* **2009**, *42*, 1660-1668.

[39] R. Shannon, *Acta Crystallogr., Sect. A* **1976**, *32*, 751-767.

[40] M. Sorai, *Top. Curr. Chem.* **2004**, *235*, 153-170.

[41] M. Sorai, Y. Nakazawa, M. Nakano, Y. Miyazaki, *Chem. Rev.* **2013**, *113*, PR41-122.

[42] T. Nakamoto, Z.-C. Tan, M. Sorai, *Inorg. Chem.* **2001**, *40*, 3805-3809.

[43] N. Wannarit, O. Roubeau, S. Youngme, P. Gamez, *Eur. J. Inorg. Chem.* **2013**, *2013*, 730-737.

[44] M. Sorai, S. Seki, *J. Phys. Chem. Solids* **1974**, *35*, 555-570.

[45] Z. Arcis-Castíllo, S. Zheng, M. A. Siegler, O. Roubeau, S. Bedoui, S. Bonnet, *Chem., Eur. J.* **2011**, *17*, 14826-14836.

[46] N. Ortega-Villar, M. Muñoz, J. Real, *Magnetochemistry* 2016, *2*, 16.

[47] V. Ksenofontov, A. B. Gaspar, V. Niel, S. Reiman, J. A. Real, P. Gütlich, *Chem., Eur. J.* **2004**, *10*, 1291-1298.

[48] J. A. Real, I. Castro, A. Bousseksou, M. Verdaguer, R. Burriel, M. Castro, J. Linares, F. Varret, *Inorg. Chem.* **1997**, *36*, 455-464.

[49] M. H. Klingele, B. Moubaraki, J. D. Cashion, K. S. Murray, S. Brooker, *Chem. Commun.* **2005**, 987-989.

[50] S. Bonnet, M. A. Siegler, J. S. Costa, G. Molnar, A. Bousseksou, A. L. Spek, P. Gamez, J. Reedijk, *Chem. Commun.* **2008**, 5619-5621.

[51] G. Aromi, C. M. Beavers, J. Sanchez Costa, G. A. Craig, G. Minguez Espallargas, A. Orera, O. Roubeau, *Chem. Sci.* **2016**, *7*, 2907-2915.

[52] B. Schneider, S. Demeshko, S. Dechert, F. Meyer, *Angew. Chem. Int. Ed.* **2010**, *49*, 9274-9277.

[53] V. Gómez, C. Sáenz de Pipaón, P. Maldonado-Illescas, J. C. Waerenborgh, E. Martin, J. Benet-Buchholz, J. R. Galán-Mascarós, *J. Am. Chem. Soc.* **2015**, *137*, 11924-11927.

[54] M. Quesada, F. Prins, E. Bill, H. Kooijman, P. Gamez, O. Roubeau, A. L. Spek, J. G. Haasnoot, J. Reedijk, *Chem., Eur. J.* **2008**, *14*, 8486-8499.

[55] J.-B. Lin, W. Xue, B.-Y. Wang, J. Tao, W.-X. Zhang, J.-P. Zhang, X.-M. Chen, *Inorg. Chem.* **2012**, *51*, 9423-9430.

[56] S. Decurtins, P. Gutlich, K. M. Hasselbach, A. Hauser, H. Spiering, *Inorg. Chem.* **1985**, *24*, 2174-2178.

[57] A. Hauser, *Top. Curr. Chem.* **2004**, *234*, 155-198.

[58] J.-F. Letard, *J. Mater. Chem.* **2006**, *16*, 2550-2559.

[59] M. Darawsheh, G. Aromi, O. Roubeau, *unpublished results.*

[60] *SAINT and SADABS*, Bruker AXS Inc., Madison, Wisconsin, USA.

[61] G. M. Sheldrick, *Acta Cryst. A* **2015**, *71*, 3-8.

The three magnetic states, [LS–LS], [LS–HS] and [HS–HS], of a dinuclear Fe(II) supramolecular helicate may be accessed *via* thermal or chemical changes, solvate-molecules exchange or light irradiation.

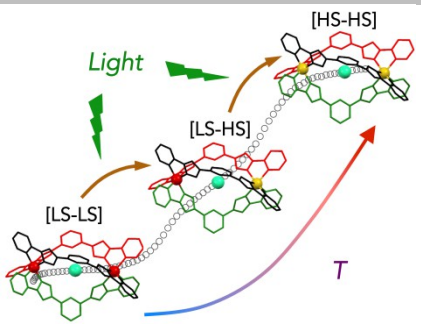

M. Darawsheh, L. A. Barrios, O. Roubeau, S. J. Teat and G. Aromí**

Page No. – Page No.

Guest, Light and Thermally Modulated Spin Crossover in $[Fe(II)_2]$ Supramolecular Helicates